Experimental study of the halo nucleus ^{6}He using the ^{6}Li(γ, π^+)^{6}He reaction

N. P. Harrington,[1] D. Branford,[1,*] K. Föhl,[1] E. Roche,[1] J. R. M. Annand,[2] R. Beck,[3] P. Grabmayr,[4] T. Hehl,[4] D. Hornidge,[3] K. Livingston,[2] J. C. McGreorge,[2] I. J. D. MacGregor,[2] I. Martin,[4] K. Monstad,[2] F. Moschini,[4] A. Reiter,[3] S. Waddell,[2] D. P. Watts,[2] and S. Young[5]

[1]*School of Physics, University of Edinburgh, Edinburgh EH9 3JZ, United Kingdom*
[2]*Department of Physics and Astronomy, University of Glasgow, Glasgow G12 8QQ, United Kingdom*
[3]*Institut für Kernphysik, Johannes-Gutenberg Universität, D-55099 Mainz, Germany*
[4]*Physikalische Institut, Universität Tübingen, D-72076 Tübingen, Germany*
[5]*Department of Physics, University of Surrey, Guildford GU2 7HX, United Kingdom*

(Received 11 December 2006; revised manuscript received 27 February 2007; published 24 April 2007)

The reaction ^{6}Li(γ, π^+)^{6}He was studied over the angular range $\theta_\pi = 40$–150° with the aim of investigating the halo structure of ^{6}He. Photons from a bremsstrahlung beam were tagged in the energy range $E_\gamma = 170$–220 MeV at a resolution of $\Delta E_\gamma = 630$ keV, and positively charged pions detected using high resolution stacked HpGe detectors. The measured angular distributions for the resolved ^{6}He ground and 1.80 MeV excited states are compared to previous measurements and theoretical calculations based on the impulse approximation. It is deduced that the ground state rms radius of the ^{6}He nucleus may be larger than previously thought and that the first excited 1.80 MeV state may also be a halo state.

DOI: 10.1103/PhysRevC.75.044311 PACS number(s): 24.10.Eq, 25.20.Lj, 27.20.+n

I. INTRODUCTION

Halo nuclei are light nuclei that occur on the chart of the nuclides in regions close to the limits at which nuclei become unstable to either proton or neutron emission. They are characterized by having either a small neutron or proton separation energy (S_n and S_p, respectively), and these give rise, respectively, to n- and p-tails in the density distribution that extend far beyond the central nuclear core [1,2]. Hence, the halo nuclei can be modelled as a core of dense nuclear matter surrounded by one or two weakly coupled nucleons that give rise to the halo [3]. Typically, the halos are comparable in size to Pb nuclei.

Studies of halo nuclei are particularly important as they give new insights into the properties of pure neutron and proton matter at very low densities compared to normal nuclear matter [2]. Halo studies are also linked to the wider issue of whether all nuclei have significant neutron skins, which could influence nuclear reaction rates, particularly at collision energies relevant to stellar burning and the formation of new elements in supernova explosions [4,5]. In addition, halo nucleus studies provide unique tests of microscopic models, cluster models, and three body theories [6–8].

Although most halo nucleus measurements have been made by studying the scattering and breakup of beams of radioactive halo nucleus ions in the strong fields surrounding heavy nuclei or inverse light-ion reactions [9–14], it was realised quite early in the history of the subject that a few halo nuclei can be accessed by (γ, π) reactions. These photonuclear reactions have the advantage of involving negligible initial state interactions and make use of the very precise electromagnetic probe. Also, the final state interactions (FSI) can be minimized by using incident photon energies such that the kinetic energies of the outgoing pions are well below the $T_\pi = 150$ MeV required to strongly excite the $\Delta(1232)$ nucleon resonance. A further advantage is that excited state halos can be excited and investigated; this being generally not possible for reactions involving radioactive beams since they γ-decay to the ground state or breakup before reaching the secondary target.

To date, of the possible reactions ^{6}Li(γ, π^+)^{6}He, ^{11}B(γ, π^+)^{11}Be, and ^{17}O(γ, π^-)^{17}F, only ^{6}Li(γ, π^+)^{6}He has been studied in some detail. The total cross section for the population of the unresolved ^{6}He ($J^\pi = 0^+$) ground and 1.80 MeV (2^+) states from the incident E_γ threshold to 7.2 MeV above threshold was measured at Saclay using the endpoint region of a bremsstrahlung beam generated from an electron beam that was stepped in E_e-energy intervals of 0.5–1.0 MeV [15]. Positively charged π-particles, which stopped in the target, were identified by observing the delayed signals from the decay $\mu^+ \rightarrow e^+ + \nu_e + \bar{\nu}_\mu$, which has a half-life of 2.6 μs. The results show a doubling of the cross section at $E_e \sim 1.9$ MeV suggesting that above this threshold the reaction leads to excitation of the first excited state with a cross section comparable to the ground state. Differential cross sections were measured at Tokyo [16] and MIT-Bates [17] using the endpoint regions of bremsstrahlung beams generated by electron beams of $E_e = 170$–195 MeV and 200 MeV, respectively. Charged particles were detected using high-resolution magnetic spectrometers which allowed a separation to be made of endpoint π^+-particles leading to the ^{6}He ground and 1.80 MeV states. Measurements were made at a number of angles relative to the beam direction, each of which corresponded to a different amount of momentum being transferred by the reaction to the nuclear system; the largest angles corresponding to the largest momentum transfers. Absolute cross sections were determined in all cases by comparing the results to measurements on a proton target and normalising to the well known $p(\gamma, \pi^+)n$ cross sections.

*Electronic address: db@ph.ed.ac.uk

The differential results were compared to distorted-wave impulse approximation (DWIA) calculations carried out in momentum space. For these calculations, it is assumed that the incident photon interacts with the valence proton of ^{6}Li to produce a π^+-particle that leaves the nucleus and a neutron that is trapped by the ^{6}He residual nucleus into an orbit associated with the halo. The ^{4}He core acts as a spectator and does not take part in the reaction process. Based on this model, the reaction cross section can be represented in momentum space by an expression of the form

$$d\sigma/d\Omega \propto \int \Psi_f^* \phi_\pi^* t_{\gamma,\pi} \Psi_i d\tau,$$

where, Ψ_i, Ψ_f^*, and ϕ_π^* are the wave functions of the struck nucleon, the final *halo nucleon*, and outgoing pion, respectively. The operator $t_{\gamma,\pi}$ is for the reaction $N(\gamma,\pi)N'$ on a free nucleon.

In considering this equation, it should be noted that the $t_{\gamma,\pi}$ operator is well known and can be represented by a sum of simple algorithms [18]. Also, well below the $\Delta(1232)$ resonance, the FSI are sufficiently small to allow reasonably accurate descriptions of ϕ_π^* to be derived using optical model parameters, or, to the accuracy of previous experimental results and those presented here, by plane waves. The wave function of the struck nucleon Ψ_i can usually be accurately determined using $(e,e'p)$ reactions to study the target nucleus [19]. A further consideration is the fact that the *halo nucleon wave function* appears fully in the reaction cross section equation, unlike in the case of many heavy-ion reactions where significant contributions to the cross section arise from interactions involving other nucleons. In addition, because the *halo nucleon wave function* appears linearly in the equation, measurements of the (γ,π) angular distributions can be considered as essentially mapping out the *halo nucleon wave function* in momentum space. It is for these reasons that (γ,π) reaction studies are considered ideal for carrying out sensitive direct tests of *halo wave functions* in halo nuclei.

The strongest evidence that ^{6}He is a halo nucleus, provided by ^{6}Li$(\gamma,\pi^+)^6$He reaction studies, comes from the MIT-Bates angular distribution measurement of Shaw *et al.* [17], which contains a cross section measurement at the backward angle $\theta_\pi = 135^\circ$. The results have been compared to several DWIA calculations which used (i) harmonic oscillator (HO) wave functions and (ii) wave functions based on a Woods-Saxon (WS) potential to describe the momentum distribution of the ^{6}He *halo neutron* produced in the reaction (e.g., Refs. [20–22]). It has since been assumed that the WS potential would give rise to a reasonable wave function to describe the halo neutron, whereas the more steeply rising HO potential would limit the spatial dimension of the wave function to a size more appropriate to that of a neutron in a non-halo nucleus [22,23]. The results of the calculations are similar at forward angles for both wave functions. However, at angles larger than $\theta_\pi = 110^\circ$, the WS cross sections are considerably larger than the HO cross sections, which can be attributed to the WS halo neutron momentum distribution being more concentrated at lower momentum values than those of the struck proton in ^{6}Li and hence providing more possibilities for higher momentum transfers to occur. In view of the result that the WS curve passes close to the cross section at $\theta_\pi = 135^\circ$ obtained by Shaw *et al.*, whereas the HO result is a factor of 5 too low, it was concluded that the ^{6}Li$(\gamma,\pi^+)^6$He results support the assumption that ^{6}He is a halo nucleus [22,23]. A more recent theoretical analysis using a realistic description of ^{6}He based on cluster wave functions reached a similar conclusion [24].

In view of the many technical advances for carrying out photonuclear reaction studies that have been made in recent years, particularly the development of tagged photons beams, we considered it timely to make a new investigation of the halo nucleus ^{6}He using the ^{6}Li$(\gamma,\pi^+)^6$He reaction. The experimental method and analysis are described in Sec. II, followed by a discussion, summary and conclusions, in Secs. III and IV, respectively.

II. EXPERIMENTAL METHOD AND ANALYSIS

Our measurement was carried out over a 6-day period at the Institut für Kernphysik, University of Mainz, Germany. A bremsstrahlung photon beam was produced by a ~15 nA beam of 855 MeV electrons from the Mainz microtron (MAMI-B) incident on a 4μm Ni radiator. Photons in the range $E_\gamma = 114$–792 MeV were analyzed using the Glasgow tagging spectrometer [25,26], which gave a tagged photon resolution and overall counting rate of typically $\Delta E_\gamma = 2$ MeV and 5×10^7 s^{-1}, respectively. Since we were interested in resolving the π^+-groups leading to the ^{6}He ground state and 1.80 MeV (2^+) state, we also used the so-called "tagging microscope", which is a second layer of more closely spaced focal plane detectors [27]. At the position used for this experiment, the microscope covered the range $E_\gamma = 170$–220 MeV at a resolution of approximately $\Delta E_\gamma = 630$ keV. The photon beam was collimated to a diameter of ~ 8 mm at the target. The ^{6}Li$(\gamma,\pi^+)^6$He measurement was made using a 1 cm thick target of 95.5% enriched ^{6}Li, which was determined by weighing to correspond to $(N_\rho)_{^6\mathrm{Li}} = 0.0383$ mol/cm^2. The target was inclined at an angle of 20° with respect to the beam direction to increase the effective target thickness relative to the beam and minimise the energy loss of π-particles in the target material. The calibration reaction $p(\gamma,\pi^+)n$ was studied for approximately 20% of the beam time using a 1 mm thick CH_2 target $[(N_\rho)_{CH_2} = 0.0143$ mol/cm$^2]$ placed at the position of the ^{6}Li target for several hours each day. The fraction of tagged bremsstrahlung photons passing through the collimator, the tagging efficiency, was measured several times and remained stable at $55 \pm 1\%$.

The kinetic energies T_π of π^+-particles produced in the target were measured by an array of HpGe detectors (The Edinburgh Ge6-Array), designed specifically for this type of experiment. Each detector consists of six individual planar HpGe detector elements, which have been assembled in a stack to produce a thick detector that subtends a solid angle of 100 msr when used with the front face 5 cm from the target as shown schematically in Fig. 1. The first two crystals of each detector had a nominal thickness of 15.0 mm and could each stop pions and protons with kinetic energies of 35 and 77 MeV, respectively. The other crystals had a nominal

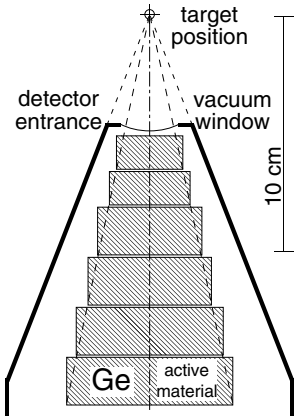

FIG. 1. Schematic diagram showing one of the five stacked HpGe detectors used in this experiment.

thickness of 20 mm and could each stop pions and protons with kinetic energies of 44 and 95 MeV, respectively. The full Ge thickness of each detector allowed pions and protons with kinetic energies up to 130 MeV and 250 MeV to be stopped, respectively. A novel feature of these detectors is the use of ultrathin electrical contacts to each element. The process to manufacture these was developed by the manufacturer to minimise energy losses in the nonactive electrical contact layers of the detector and thus reduce the contributions to the energy resolution from straggling as particles pass from one element to the next. The experimental arrangement of the detectors is shown in Fig. 2. The three detectors used

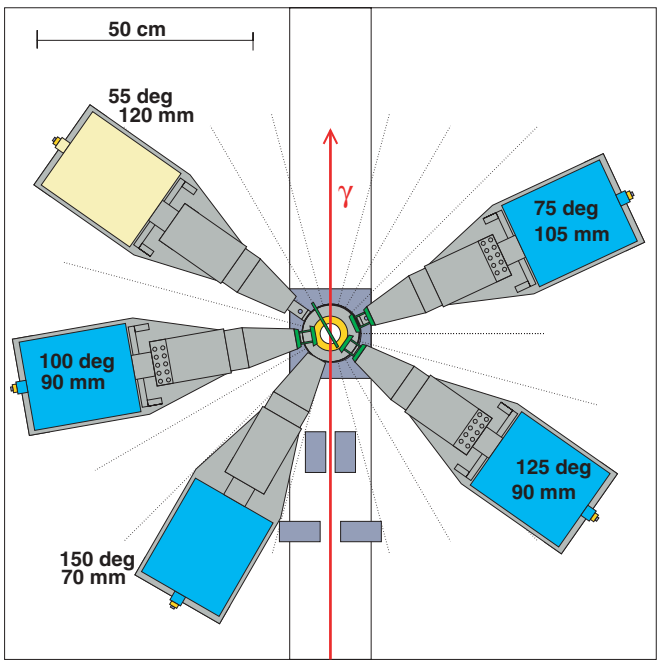

FIG. 2. (Color) Diagram of the experimental arrangement of the detectors and target on the 1.8 m × 1.8 m square correlation table. The indicated distances are from the center of the target to the front face of each detector. The target and DSSSD mountings are shown in green. The other colored regions show the dewars containing liquid N_2 used to cool the detectors.

at polar angles $\theta_\pi = 100^\circ$, 125°, and 150° relative to the beam direction, remained fixed at these angles throughout the experiment. The fourth detector shown at $\theta_\pi = 75^\circ$ was used at $\theta_\pi = 45^\circ$, 55°, 65°, and 75°, where the cross section is larger, for appropriately weighted fractions of the run period. Data from the detector used at $\theta_\pi = 55^\circ$ on the opposite side of the beam were not fully analyzed because element 1 suffered electrical breakdown approximately halfway through the experiment. However, the counting rates were included with those of the other detectors in checks of the beam intensity and position, which showed that the beam was stable throughout the experiment.

To minimize the pile up of after-pulses from μ-decays on the energy pulses, short pulses (400 ns base to base) were generated using timing filter amplifiers. Using charge-sensitive analog-to-digital-converters (QDCs), this gave a resolution measured with 1.33 MeV γs of ~30 keV in each detector element. The detectors used at $\theta_\pi = 100^\circ$ and 125°, and forward angles were each equipped with a pair of double sided Si strip detectors (DSSSDs) that were separated by 4.0 cm as shown in Fig. 2. Each DSSSD had dimensions 2.54 cm × 2.54 cm × 300 μm, and had 24 strips on each side. Adjacent pairs of horizontal strips were electrically connected together to reduce the required number of strip electronic channels. The DSSSDs were used to track particles into the stacked HpGe detectors and measure the polar and azimuthal angles of emission with an accuracy of $\Delta\theta_\pi = \pm 2^\circ$ and $\Delta\phi_\pi = \pm 4^\circ$, respectively. This was necessary to minimize the kinematic broadenings around $\theta_\pi \sim 90^\circ$ sufficiently to resolve π^+-particles leading to the ground state and 1.80 MeV states.

Timing signals were generated using leading edge discriminators and relative times recorded using time-to-digital-converters (TDCs). Each of the time peaks arising from coincidences between the HpGe detectors and the main tagger focal plane array had a full-width-half-maximum (FWHM) of ~5 ns. The QDC and TDC information was read out using the ACQU data acquisition system [28]. Events corresponding to the detection of π^+-particles were selected using ΔE versus E information and demanding that an after-pulse from the decay $\mu^+ \rightarrow e^+ + \nu_e + \bar{\nu}_\mu$ occurred within 7 μs [29]. Two types of two dimensional ΔE versus E plots were produced, corresponding to (i) ΔE signals from the strip detectors versus the full energy E deposited in the HpGe stack, and (ii) ΔE signals from the first detector in a HpGe stack versus the full energy E deposited in the stack. An example of spectrum type (ii) is shown in Fig. 3. Cuts around the pion ridges, such as shown in Fig. 3, were made to select the events of interest. Implementation of these selection procedures coupled with the requirement of an after-pulse being detected eliminated most events where the π^+-particles were stopped or lost energy through nuclear interactions with the detector material. Events in coincidence with tagged photons were selected using a time window centered around the time peak in the HpGe-tagger time spectrum. The random contribution to any spectrum was determined using events that contributed to the approximately flat backgrounds on either side of the time peak, these events being treated in an identical manner to the *true-plus-random* events in the region of the time peak.

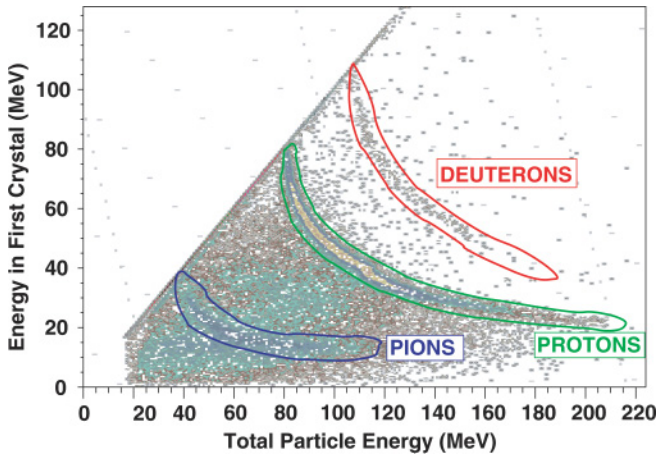

FIG. 3. (Color) Two dimensional plot of ΔE signals from the first detector versus E signals from the full detector stack obtained using events where the particles tracked into the stacked HpGe detector. The pion ridge could be more strongly enhanced with respect to the background than that shown by selecting events that had afterpulses associated with them. The lines show the cuts used to select π^+-particles, protons, and deuterons.

Calibrations of the detectors were made using events obtained with the CH_2 target. Two-dimensional (2D) plots of (i) calculated pion energies at the reaction vertex T_π^{calc} versus (ii) measured pion energies were made using for (i) the E_γ tagger information, the measured θ_π angle and two-body kinematics, and for (ii) the detector response for π^+-particles corrected to the reaction vertex using calculated energy losses. The energy losses in the target were made assuming the π-particles originated at a depth of half the target thickness. The T_π^{calc} included a 4.1 MeV contribution to account for the kinetic energy given to the μ^+-particle in the decay $\pi^+ \rightarrow \mu^+ + \nu_\mu$, which occurred within the response time of the detector electronics. These 2D plots showed distinct ridges from the $p(\gamma, \pi^+)n$ reaction, which were used to derive calibration parameters such that when these were applied to the data they produced a single ridge along the line joining points where the reconstructed pion energies equal the calculated pion vertex energies.

Based on these calibrations missing energy spectra were calculated for the $^6\text{Li}(\gamma, \pi^+)^6\text{He}$ and $p(\gamma, \pi^+)n$ reactions using the equation

$$E_m = E_\gamma + M_T - E_\pi - E_R,$$

where E_γ, M_T, E_π, and E_R are the tagged photon energy, mass of the target nucleus, total energy (mass + kinetic energy) of the π^+-particle at the reaction site, and total energy of the recoiling residual nucleus (or neutron) determined using two-body reaction kinematics, respectively.

Two examples of missing energy spectra with random counts subtracted obtained using the ^{6}Li target and one obtained using the CH_2 target are shown in Figs. 4(a), 4(b), and 4(c), respectively. Spectra observed at each θ_π using the CH_2 target showed a peak and a smoothly varying background from events associated with the $p(\gamma, \pi^+)n$ and $^{12}\text{C}(\gamma, \pi^+)^{12}\text{B}$ reactions, respectively. Fits were made to these spectra using

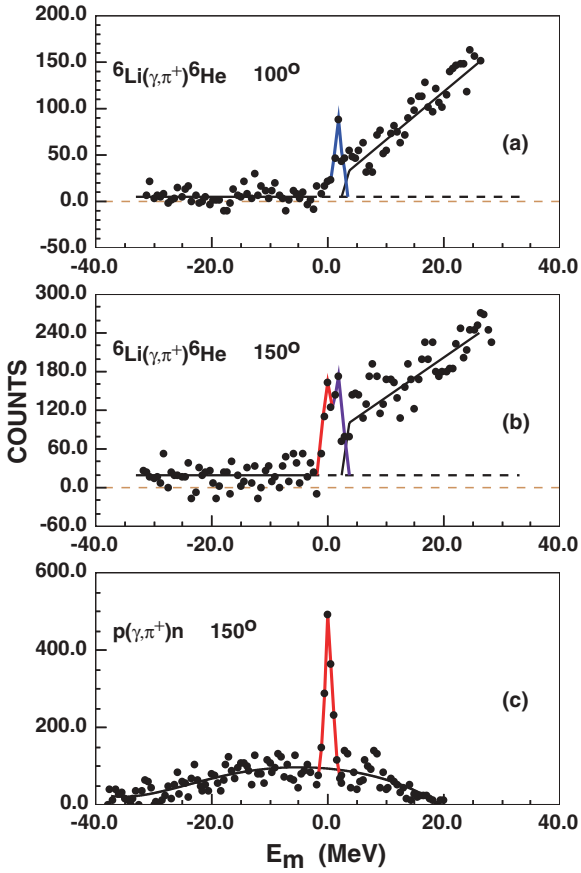

FIG. 4. (Color) Spectra for the $^6\text{Li}(\gamma, \pi^+)^6\text{He}$ and $p(\gamma, \pi^+)n$ reactions obtained at the indicated detection angles for tagged photons in the range $E_\gamma = 170$–220 MeV. The red and blue peaks shown in (a) and (b) correspond to population of the ground and 1.80 MeV states of ^{6}He, respectively. The background counts in (c) are from reactions on C in the CH_2 target.

a Gaussian shape of variable width above a background to determine the number of counts in the peak from the $p(\gamma, \pi^+)n$ reaction at each angle. An example of such a fit is shown in Fig. 4(c). From the widths of the Gaussians, it was determined that the missing energy resolution was ~1.4 MeV FWHM. It is not understood why this was larger than the expected resolution of ~1.2 MeV FWHM, but may have resulted from larger than expected dead layers between some of the detector elements. Close inspection of the 2D calibration plots indicated a few slight discontinuities in the ridges at energies close to those corresponding to crystal boundaries. The cause of these has been subsequently traced to detector elements that were only just fully depleted at the recommended bias voltages. For future measurements, we intend to slightly overbias these elements in the hope that this will improve the detector resolutions.

Fits to the $^6\text{Li}(\gamma, \pi^+)^6\text{He}$ spectra at each θ_π were made by first considering the regions corresponding to negative values of E_m. We attributed some of the counts in these regions to interactions with the air, which since the Q-values involved are quite different from that for the $^6\text{Li}(\gamma, \pi^+)^6\text{He}$ reaction, are expected, when analyzed using E_R calculated

with ^{6}Li$(\gamma, \pi^+)^6$He kinematics, to give rise to broad smeared out distributions similar to that for the C contribution to Fig. 4(c). Events in the negative E_m regions will also arise from the ~3% pions (both π^+ and π^-) that undergo the decay $\pi \rightarrow \mu + \nu$ in flight ($\tau = 26$ ns, Q = +33.8 MeV) followed by an after-pulse from the decay $\mu^+ \rightarrow e + 2\nu$ ($\tau = 2.2$ μs). GEANT [30] simulations of the response of a solid state detector to events of this type arising from monoenergetic π^+- and π^--particles show broad peaks spread out over many tens of MeV that extend from low energies to ~20 MeV above T_π [31]. Based on these considerations and the fact that the statistics are poor in the negative E_m regions, we considered it reasonable to fit the negative E_m data with a flat line. This was extrapolated under the peaks and obviously with less reliability into regions of higher ^{6}He excitation. The larger background observed for the $\Theta_\pi = 150^\circ$ spectrum is attributed to events from the downstream column of air that could not be rejected by tracking because the detector at 150° was not instrumented with strip detectors.

Fits to the ^{6}Li peaks were made using two Gaussian peaks above the background with widths of 1.4 MeV FWHM centered in the missing energy plots at $E_m = 0.00$ and 1.80 MeV. Counts in the region above $E_m = 1.86$ MeV, which correspond to excitation of continuum ^{6}He above the neutron breakup threshold, were fitted by sloping lines. The cut off at 1.86 MeV was smeared by the resolution. Following a study of the related reaction ^{7}Li$(\gamma, p)^6$He [32], it was suggested that a broad excited state exists at $E_x = \sim 5$ MeV in the neutron breakup continuum of ^{6}He. However, even if such a state were to be excited by the ^{6}Li$(\gamma, \pi^+)^6$He reaction with a similar cross section, the statistical accuracy of the present experiment would not be sufficient for it to be observed. In view of this, we consider it reasonable to use a straight line fit to the continuum region, which in any case has only a minor influence on the fits to the ground state and 1.80 MeV peaks. Examples of the full fits are shown in Figs. 4(a) and 4(b). Based on the fits to all the spectra, the numbers of counts associated with the ^{6}Li$(\gamma, \pi^+)^6$He reaction leading to the ground and 1.80 MeV states were determined at each angle.

Cross sections were obtained at each laboratory angle using the equation

$$\left(\frac{d\sigma}{d\theta}\right)_{\mathrm{Li}} = \frac{2(\epsilon_\pi)_H}{(\epsilon_\pi)_{\mathrm{Li}}} \frac{N_{\mathrm{Li}}}{N_{\mathrm{H}}} \frac{(N_\rho)_{\mathrm{CH_2}}}{(N_\rho)_{^6\mathrm{Li}}} \frac{Q_{\mathrm{CH_2}}}{Q_{\mathrm{Li}}} \left(\frac{d\sigma}{d\theta}\right)_{\mathrm{H}},$$

where the 2 arises because there are two hydrogen atoms in each CH_2 molecule, N_{Li} and N_{H} were the number of counts in the peaks from the reactions on Li and hydrogen, respectively, $(\epsilon_\pi)_{\mathrm{Li}}$ and $(\epsilon_\pi)_{\mathrm{H}}$ were the fractions of π^+-particles from the Li and CH_2 targets that did not undergo nuclear reactions in the HpGe detectors, respectively, Q_{Li} and $Q_{\mathrm{CH_2}}$ are the total number of photons that passed through the Li and CH_2 targets, respectively, and $(\frac{d\sigma}{d\theta})_{\mathrm{H}}$ is the laboratory differential cross section for the $p(\gamma, \pi^+)n$ reaction. Values for $(\frac{d\sigma}{d\theta})_{\mathrm{H}}$ in the center-of-mass frame were obtained using the MAID code developed at the University of Mainz [33], and these were subsequently transformed into the laboratory frame of reference using the appropriate Jacobian as given for example in Ref. [34]. The function ϵ_π vs T_π was obtained by studying, as a function of increasing tagged photon energy, the falloff in yield of π^+-particles from the reaction $p(\gamma, \pi^+)n$ compared to variations in the relative numbers predicted to be incident on the detector as deduced from MAID cross section calculations.

TABLE I. Table of differential cross sections at the indicated laboratory angles. The second column shows calculated results obtained using the MAID code transformed into the laboratory reference frame. Columns 3 and 4 show the results of the present experiment for the ^{6}Li$(\gamma, \pi^+)^6$He reaction leading to the 0^+ ground state and 2^+ 1.80 MeV states of ^{6}He, respectively. The errors shown include both statistical and systematic errors.

Angle deg	$d\sigma/d\Omega$ (Calc.) $p(\gamma, \pi^+)n$ μb sr^{-1}	$d\sigma/d\Omega$ (Exp.) ^{6}Li$(\gamma, \pi^+)^6$He$_{\mathrm{g.s.}}$ μb sr^{-1}	$d\sigma/d\Omega$ (Exp.) ^{6}Li$(\gamma, \pi^+)^6$He(1.80) μb sr^{-1}
45	10.54	1.333 ± 0.257	0.818 ± 0.223
55	10.21	0.859 ± 0.121	0.402 ± 0.089
65	9.84	0.490 ± 0.080	0.336 ± 0.070
75	9.36	0.176 ± 0.057	0.441 ± 0.072
100	7.75	0.012 ± 0.105	1.379 ± 0.134
125	6.29	0.258 ± 0.067	0.697 ± 0.090
150	5.30	0.810 ± 0.098	0.795 ± 0.090

Results obtained using the above equation are presented in Table I. The errors in the experimental results include statistical errors associated with the peak and background fits, a ±3% error associated with the ϵ_π and a 5% systematic error associated with the data against which the MAID calculations were tested [35]. These errors were added in quadrature. Due to the poor statistical accuracy of the new measurement, the determination of the numbers of counts in the ^{6}He ground and 1.80 MeV peaks relied heavily on the detector calibrations, which we estimate were accurate to approximately ±100 keV. To investigate possible further systematic errors that could arise from this, we studied the effect of varying the calibrations by ±100 keV. This gave average changes of ±6% in the peak intensities, which were added in quadrature to the other errors and are included in the results shown in Table I.

III. DISCUSSION

Figure 5 shows the results presented in Table I compared to previous measurements of the ^{6}Li$(\gamma, \pi^+)^6$He cross sections and theoretical calculations. The dashed and long-dashed curves show, respectively, the results of DWIA calculations for excitation of the ^{6}He ground state based on HO and WS single particle wave functions [23], which were carried out to investigate the significance of the experimental results of Shoda *et al.* [16] to the halo structure of ^{6}He. The solid curve is the result of a PWIA calculation based on cluster wave functions [24] that was made prior to the present experiment specifically for comparison with our new measurement. From Fig. 5 it is evident that our forward angle results for the reaction leading to the ^{6}He ground state are in reasonable agreement with previous measurements. Also, our result at $\theta_\pi = 100^\circ$ supports the existence of a deep minimum in the cross section in the vicinity of $\theta_\pi = 100^\circ$ as indicated by the neighboring experimental points from Shoda *et al.* [16] and

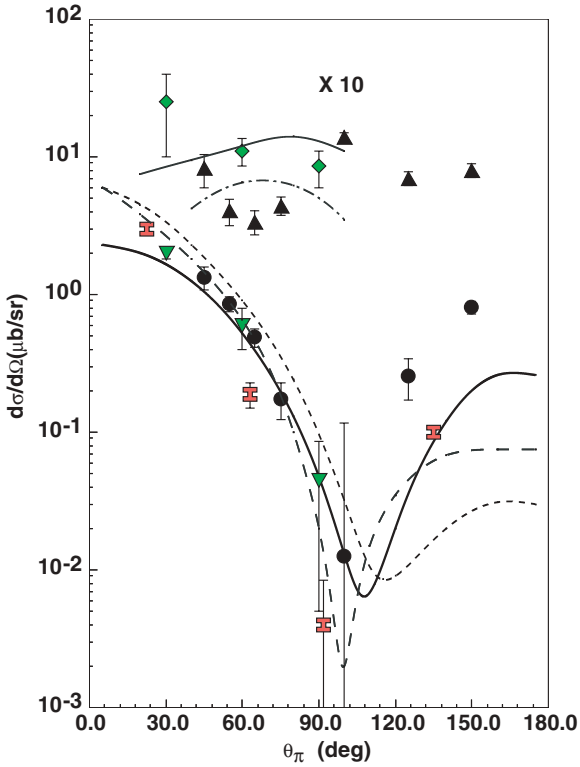

FIG. 5. (Color) Differential cross section measurements for the ^{6}Li$(\gamma, \pi^+)^6$He reaction leading to the ground and 1.80 MeV ($\times$10) states. Solid black circles and triangles are from this experiment. Green inverted triangles and diamonds, and the red I symbols are from Shoda *et al.* [16] and Shaw *et al.* [17], respectively. The dashed and long-dashed curves compared to the ground state data are DWIA calculations based on harmonic oscillator and Woods-Saxon single particle wave functions [23], respectively. The solid curve is a more recent PWIA calculation based on cluster wave functions, that was made prior to the present measurement for comparison with the new data [24]. The solid and dot-dashed curves compared to the 1.80 MeV state data are DWIA calculations [16] based on Cohen-Kurath wave functions and single particle shell model states that have been phenomenologically adjusted to electron scattering data [43], respectively.

Shaw *et al.* [17]. On the other hand, our results at $\theta_\pi = 125^\circ$ and 150° suggest that the cross section in the region of the backward angles is approximately a factor of 5 higher than previously assumed from the single backward angle data point of Shaw *et al.* In considering this disagreement, we note that the previous measurement was based on the less reliable bremsstrahlung endpoint method, and the spectrum shown in the publication does not exhibit a well-defined endpoint for either excitation of the ^{6}He ground state or 1.80 MeV state. Also, a 0.014 radiation length tantalum foil radiator was introduced 10 cm upstream of the target for the $\theta_\pi = 90^\circ$ and 130° measurements, which resulted in the ratio of real photons to calculated virtual photons for the backward angle measurements ($R = 1.03$) being very different from those at forward angles ($R = 0.09$). On the other hand, our backward angle data points were measured simultaneously with those at forward angles under identical running conditions. Also, peaks from the ^{6}Li$(\gamma, \pi^+)^6$He and calibration $p(\gamma, \pi^+)n$ reactions were clearly observed in our data. In view of these results, we consider the new backward angle results to be more reliable than the data point of Shaw *et al.* and therefore only consider these in the following discussion.

From Fig. 5 it is evident that all the theory curves are in reasonable agreement with the experimental data at forward angles and reproduce the strong minimum at $\theta_\pi \sim 100^\circ$. This supports the assumption that the reaction proceeds through an initial interaction with the valence $1p$-shell proton in ^{6}Li and can be well described by DWIA calculations in which the ^{4}He core acts as a spectator. The differences in the backward angle behavior of the calculations show the sensitivity of the cross section in this region to the radial extent of the halo wave function; larger backward angle cross sections corresponding to physically more extensive halos. As discussed earlier here, the calculations of Karatiglides [23] based on HO wave functions, which suppress the formation of a halo, give results considerably below the backward angle data whereas calculations based on Woods-Saxon wave functions which give rise to a halo are closer to the experimental data. The more recent PWIA calculations by Young [24], based on state-of-the-art cluster wave functions which describe well the mean square radius of ^{6}He determined using radioactive beam breakup reactions, produce even higher backward angle cross sections. However, although these calculated results agree well with the data point of Shaw *et al.*, they fall significantly below the new backward angle data.

Based on the above considerations, the fact that our new $\theta = 125^\circ$ and 150° data points lie above the theoretical curves of Young suggests that either the ^{6}He halo extends to a larger radius than presently assumed or the reaction model breaks down in regions corresponding to higher transferred momenta. At E_γ comparable to those used here, the theoretical descriptions of photonuclear cross sections usually require the inclusion of mechanisms to account for the absorption of photons on nucleon pairs, exchanged pions and medium modifications to the intermediate excitation of isobars [36–40]. However, the total cross section per nucleon at $E_\gamma \sim 200$ MeV for photodisintegration of the deuteron, which is a reaction on low density nuclear matter closely related to the ^{6}Li$(\gamma, \pi^+)^6$He reaction, is only ~15% higher than that for pion production from the proton [41]. This suggests that effects such as absorption on nucleon pairs, exchange particles and medium modifications to intermediate isobar excitation may not be important for the ^{6}Li$(\gamma, \pi^+)^6$He reaction at $E_\gamma \sim 200$ MeV. In addition, Fix and Ahrenövel [42] have studied the effects of NN and πN rescattering on $d(\gamma, \pi)$ cross sections. Extrapolating their results for the $d(\gamma, \pi^+)nn$ channel to $E_\gamma = 200$ MeV indicates that πN rescattering leads to an increase of ~15% in the cross section compared to the $p(\gamma, \pi^+)n$ impulse approximation result. In view of these results, we consider it unlikely that large contributions to the cross section arise from these other mechanisms and hence conclude that the most likely explanation of the fact that the new backward angle data points lie well above the calculation of Young is that the ^{6}He halo extends to a larger radius than assumed in that calculation. Clearly, new calculations should be made to investigate this more thoroughly and in particular check if the

data can be fitted with halo wave functions that have a larger rms radius yet still remain realistic.

Figure 5 also shows the new data for the ^{6}Li$(\gamma,\pi^+)^6$He reaction leading to the 2^+ first excited state at 1.80 MeV, compared to the previous measurement of Shoda *et al.* [16] and theoretical calculations. The solid and dot-dashed curves show the results of DWIA calculations based on Cohen-Kurath wave functions [16] and single particle shell model states that have been phenomenologically adjusted to electron scattering data [43], respectively. Except at $\theta_\pi \sim 60^\circ$, the new data compare reasonably well with the forward angle results of Shoda *et al.* and provide the first information on the behavior of the cross section at backward angles. Using the sum of our cross section results multiplied by $\sin\theta_\pi$ to estimate angle-integrated cross sections over the range $\theta_\pi = 45$–150°, we obtained a result for population of the 1.80 MeV state relative to the ground state of $R(1.80/0.00) = 1.37 \pm 0.27$. This is in general agreement with the much earlier Saclay result [16] remarked on here in Sec. I. There is no evidence for a deep diffraction minimum in this first excited state angular distribution as may be expected due to the incoherent addition of cross sections from transitions connecting $M = 0$ and ±1 substates of the initial $J^\pi = 1^+$ ^{6}Li state to the $M = 0, \pm1$ and ±2 substates of the final $J = 2^+$ ^{6}He state. Although both sets of DWIA calculations [16,43] agree reasonably well with the data, the fact that the calculations do not extend to backward angles precludes drawing quantitative conclusions regarding the halo nature of the state. Clearly it would be advantageous to have theoretical calculations to cover this angular region. However, it should be noted that the magnitudes of the cross section both at forward and backward angles are very similar to those of the ground state. Based on this information it is reasonable to conclude that the 1.80 MeV state of ^{6}He is also a halo state with a halo mean square radius comparable to that of the ground state. Although the existence of halos on excited states is not unexpected, especially for a state such as the ^{6}He 1.80 MeV level, which lies only 60 keV below S_n, these data possibly provide the first direct evidence for such states.

IV. SUMMARY AND CONCLUSIONS

In summary, we have demonstrated that a study of the halo nucleus ^{6}He through measurements on the ^{6}Li$(\gamma,\pi^+)^6$He reaction is possible within a reasonable running period using state of the art stacked HpGe detectors and tagged photons covering the region $E_\gamma = 170$–200 MeV. Although the resolution of the experiment ($\Delta E_m \sim 1.4$ MeV) was only just sufficient to resolve the peaks from π^+-particles leading to the ground $J^\pi = 0^+$ and 1.80 MeV 2^+ states of ^{6}He and the statistical accuracy of the results was only moderately good, the experiment provided valuable new information on the π^+-angular distributions, particularly at backward angles, which is the region most sensitive to the spatial extent of the halo wave function. Cross section results for the 1.80 MeV excited state at backward angles are presented for the first time. The new data on both states are in reasonable agreement with previous measurements and theoretical predictions except for the ^{6}He ground state backward angle cross sections, which are a factor $\sim$5 higher than the data point of Shaw *et al.* and the most recent PWIA calculations. From a consideration of this result, it is suggested that the rms radius of the *halo nucleons* associated with the ^{6}He ground state may be larger than previously considered. Based on the observation that the forward and backward angle cross sections for the ^{6}Li$(\gamma,\pi^+)^6$He reaction leading to the ^{6}He ground state and 1.80 MeV state are similar in magnitude, it is suggested that the 1.80 MeV state may also be a halo state. Although excited halo states are not unexpected, these new results may provide the first direct evidence for such states.

Despite the satisfactory outcome of this experiment, there is clearly a need for higher resolution better statistics measurements and more detailed theoretical investigations. On the experimental side we consider it would be worthwhile to investigate how the angular distributions change as a function of E_γ to establish that the pion FSI are really under control. Theoretically, the magnitude of effects associated with absorption on nucleon pairs, exchange currents, short range correlations, two step processes, interactions with the core, etc. should be investigated to ensure that they really are small as assumed in the present impulse-approximation calculations. It is hoped that at the conclusion of these future investigations, it will be possible to realize the full potential of investigating halo nuclei using (γ,π) reactions and make detailed accurate measurements of *halo nucleon wave functions* in the cases where this is possible.

ACKNOWLEDGMENTS

The support of the U.K. Engineering and Physical Sciences Research Council through the provision of research grants and the Ph.D. studentships of N.P.H., K.M., and S.W. is gratefully acknowledged. This work was supported in part by the EU integrated infrastructure initiative hadron physics project under contract no. RII3-CT-2004-506078, and the German DFG through grants Gr1084/7-1 and GRK 693.

[1] P. G. Hansen, A. S. Jensen, and B. Jonson, Annu. Rev. Nucl. Part. Sci. **45**, 591 (1995).
[2] I. Tanihata, J. Phys. G: Nucl. Part. Phys. **22**, 157 (1996).
[3] I. Tanihata *et al.*, Phys. Rev. Lett. **55**, 2676 (1985).
[4] V. D. Efros, W. Balogh, H. Herndl, R. Hofinger, and H. Oberhummer, Z. Phys. A **355**, 101 (1996).
[5] J. Görres, H. Herndl, I. J. Thompson, and M. Wiescher, Phys. Rev. C **52**, 2231 (1995).
[6] A. Csoto, Phys. Rev. C **48**, 165 (1993).
[7] M. V. Zhukov, B. V. Danilin, D. V. Federov, J. M. Bang, I. J. Thompson, and J. S. Vaagen, Phys. Rep. **231**, 151 (1993).
[8] Yu. F. Smirnov and Yu. M. Tchuvil'sky, Phys. Rev. C **15**, 84 (1977).
[9] N. Takigawa, M. Ueda, M. Kuratani, and H. Sagawa, Phys. Lett. **B288**, 244 (1992).

[10] I. Tanihata, D. Hirata, T. Kobayashi, S. Shimoura, K. Sugimoto, and H. Toki, Phys. Lett. **B289**, 261 (1992).
[11] T. Aumann, L. V. Chulkov, V. N. Pribora, and M. H. Smedberg, Nucl. Phys. **A640**, 24 (1998).
[12] G. D. Alkhazov *et al*., Phys. Rev. Lett. **78**, 2313 (1997).
[13] T. Aumann *et al*., Phys. Rev. C **59**, 1252 (1999).
[14] L. Giot *et al*., Phys. Rev. C **71**, 064311 (2005).
[15] G. Audit *et al*., Phys. Rev. C **15**, 1415 (1977).
[16] K. Shoda, O. Sasaki, and T. Kohmura, Phys. Lett. **B101**, 124 (1981).
[17] J. Shaw *et al*., Phys. Rev. C **43**, 1800 (1991).
[18] I. Blomqvist and J.-M. Laget, Nucl. Phys. **A280**, 405 (1977).
[19] S. Karataglidis, B. A. Brown, K. Amos, and P. J. Dortmans, Phys. Rev. C **55**, 2826 (1997).
[20] B. C. Doyle, *Excited Baryons 1988* (World Scientific, Singapore, 1989), p. 373.
[21] C. Bennhold, L. Tiator, and L. E. Wright, results presented in Shaw *et al*. [17] (1991) (unpublished elsewhere).
[22] C. Bennhold, L. Tiator, and L. E. Wright, Invited talk presented at the Workshop on the Future of the MAX-lab, 10–12 March 1997, Lund, Sweden (unpublished).
[23] S. Karataglidis, P. J. Dortmans, K. Amos, and C. Bennhold, Phys. Rev. C **61**, 024319 (2000).
[24] S. Young, Ph.D. thesis (unpublished), University of Surrey, U.K. (2004).
[25] I. Anthony *et al*., Nucl. Intrum. Methods Phys. Res. A **301**, 230 (1991).
[26] S. J. Hall *et al*., Nucl. Intrum. Methods Phys. Res. A **368**, 698 (1966).
[27] A. Reiter *et al*., Eur. Phys. J. A **30**, 461 (2006).
[28] J. R. M. Annand and B. Oussena, Nucl. Intrum. Methods Phys. Res. A **330**, 220 (1993); J. R. M. Annand, I. Anthony, and B. Oussena, *ibid*. **368**, 385 (1996).
[29] D. Branford *et al*., Phys. Rev. C **66**, 015208 (2002).
[30] R. Brun, M. Hansroul, and J. C. Lassalle, GEANT User's Guide DD/EE/82 CERN (1982).
[31] J. A. MacKenzie, Ph.D. thesis (unpublished), University of Edinburgh, U.K. (1995).
[32] M. J. Boland *et al*., Phys. Rev. C **64**, 031601(R) (2001).
[33] D. Drechsel *et al*., Nucl. Phys. **A645**, 145 (1999).
[34] L. Tiator and L. E. Wright, Phys. Rev. C **30**, 989 (1984).
[35] K. Buechler *et al*., Nucl. Phys. **A570**, 580 (1994).
[36] J. Ryckebusch, K. Heyde, L. Machenil, D. Ryckbosch, M. Vanderhaeghen, and M. Waroquier, Phys. Rev. C **46**, R829 (1992).
[37] J. Ryckebusch, D. Debruyne, W. Van Nespen, and S. Janssen, Phys. Rev. C **60**, 034604 (1999).
[38] D. Branford *et al*., Phys. Rev. C **63**, 014310 (2000).
[39] S. A. Morrow *et al*., Phys. Rev. C **71**, 014607 (2005).
[40] S. A. Morrow *et al*., Phys. Rev. C **73**, 044611 (2006).
[41] M. MacCormick *et al*., Phys. Rev. C **53**, 41 (1996).
[42] A. Fix and H. Ahrenhövel, Phys. Rev. C **72**, 064005 (2005).
[43] J. C. Bergstrom, Phys. Rev. C **21**, 2496 (1980).